

Relativistic corrections in $(e, e'p)$ knockout reactions

A. Meucci, C. Giusti, and F. D. Pacati

*Dipartimento di Fisica Nucleare e Teorica dell'Università, Pavia
and Istituto Nazionale di Fisica Nucleare, Sezione di Pavia, Italy*

(November 5, 2018)

A consistent comparison between nonrelativistic and relativistic descriptions of the $(e, e'p)$ reaction is presented. We use the nonrelativistic DWEEPY code and develop a fully relativistic model starting from the effective Pauli reduction for the scattering state and the relativistic mean field theory for the bound state. Results for the $^{16}\text{O}(e, e'p)$ differential cross section and structure functions are compared in various kinematical conditions. A limit in energy of the validity of the nonrelativistic approach is established. The effects of spinor distortion and of the effective momentum approximation for the scattering state are discussed. A satisfactory agreement with data of differential cross sections, structure functions, and polarization observables is achieved.

PACS numbers: 25.30.Fj, 24.10.Jv, 24.70.+s.

I. INTRODUCTION

Exclusive $(e, e'p)$ knockout reactions represent a very clean tool to explore the single-particle (s.p.) aspects of nuclear structure revealing the properties of proton-hole states contained in the hole spectral function [1–4].

Several high-resolution experiments were carried out at Saclay [1,5] and NIKHEF [6]. The analysis of the missing energy and momentum dependence of the experimental cross sections allowed to assign specific quantum numbers and spectroscopic factors to the peaks in the energy spectrum. The calculations for this analysis were carried out with the program DWEEPY [7], within the theoretical framework of a nonrelativistic distorted wave impulse approximation (DWIA), where final-state interactions (FSI) and Coulomb distortion of the electron wave functions are taken into account. Phenomenological ingredients were used to compute bound and scattering states. The outgoing nucleon scattering wave functions are eigenfunctions of an optical potential determined through a fit to elastic nucleon-nucleus scattering data including cross sections and polarizations. Bound-state wave functions were calculated with a Woods-Saxon well, where the radius was determined to fit the experimental momentum distributions and the depth was adjusted to give the experimentally observed separation energy of the bound final state. This theoretical approach was able to describe, with a high degree of accuracy, in a wide range of nuclei and in different kinematics, the shape of the experimental momentum distributions at missing-energy values corresponding to specific peaks in the energy spectrum. In order to reproduce the size of the experimental cross sections, the normalization of the bound-state wave function was fitted to the data and identified with the spectroscopic factor. These values, however, are smaller than those predicted by many-body theories.

Similar models based on a fully relativistic DWIA (RDWIA) framework were developed in more recent years [8–14]. In these approaches the bound nucleons are described by s.p. Dirac wave functions in the presence of scalar and vector potentials fitted to the ground-state properties of the nucleus, and the scattering wave function is solution of the Dirac equation with relativistic optical potentials obtained by fitting elastic proton-nucleus scattering data. Some of these approaches include also an exact treatment of the Coulomb distortion of the electron waves [9,10]. Also RDWIA analyses were able to give a good description of the experimental momentum distributions. Thus, the shape of the distributions in DWIA and RDWIA calculations are similar, while the spectroscopic factors, obtained by scaling the calculated cross sections to the data, are in RDWIA about 10 – 20% larger than in DWIA analyses, and thus closer to theoretical predictions. The difference was attributed to the relativistic optical potential, which leads to stronger absorption. The nucleon-nucleus interaction exhibits characteristic non-localities which arise quite naturally in the Dirac approach and whose effect was not included in standard nonrelativistic DWIA calculations, but can be accounted for in the nonrelativistic treatment by a renormalization of the scattering wave function. The so-called Darwin normalization factor [15], that essentially changes the Schrödinger wave function into the upper component of the Dirac wave function, increases the absorption due to FSI and produces a quenching of the calculated cross section by about 15%, with a corresponding enhancement of the spectroscopic factor in agreement with the results obtained in RDWIA.

New data have recently become available from TJNAF. The cross section for quasielastic $1p$ -shell proton knockout has been measured and the response functions and the asymmetry have been extracted in the $^{16}\text{O}(e, e'p)$ reaction at four-momentum transfer squared $Q^2 = 0.8$ $(\text{GeV}/c)^2$ and energy transfer $\omega \sim 439$ MeV [16]. In the same kinematics

also first polarization transfer measurements have been carried out for the $^{16}\text{O}(\bar{e}, e'p)$ reaction [17]. The polarization of the ejected proton in the $^{12}\text{C}(e, e'p)$ reaction has been measured at Bates with $Q^2 = 0.5 (\text{GeV}/c)^2$ and outgoing-proton energy $T_p = 274 \text{ MeV}$ [18].

The analysis of these new data in kinematic conditions inaccessible in previous experiments, where Q^2 was less than $0.4 (\text{GeV}/c)^2$ and T_p generally around 100 MeV, requires a theoretical treatment where all relativistic effects are carefully and consistently included. Indeed these recent data are well described by RDWIA calculations [14,16–18].

Fully relativistic models based on the RDWIA have been developed by different groups [8–14]. It was shown in Ref. [12] that the hadronic part of the relativistic transition amplitude can be written in terms of Schrödinger-like wave functions for bound and scattering states and of an effective nuclear current operator which contains the Dirac potentials. In this way, complications due to the solution of the Dirac equation can be avoided and spinor distortion can be accounted for solving a relativized Schrödinger equation, of the same type as that solved in ordinary nonrelativistic DWIA calculations with nonrelativistic or relativistic equivalent potentials, but Dirac scalar and vector potentials appear in the nuclear current operator. This so-called effective Pauli reduction does not represent an approximation. It is in principle exact and can be considered an alternative fully relativistic approach.

This approach was adopted in Refs. [19,20] with an effective momentum approximation (EMA) to incorporate spinor distortion into the effective current operator. In this approximation the momentum operators in the term $\sigma \cdot p$, appearing in the lower components of the Dirac spinor and in the effective current operator, are replaced by their asymptotic values. This model contains approximations, but accounts for all the main relativistic effects and is able to give a good description of the most recent experimental results. The spectroscopic factor extracted in comparison with $^{16}\text{O}(e, e'p)$ data for $1p$ -shell proton knockout is the same as in other RDWIA analyses, i.e. 0.7 [16].

Both nonrelativistic DWIA and RDWIA models are able to describe, with a good degree of accuracy, the $(e, e'p)$ data at low energies, but the nonrelativistic DWIA approach is more flexible. Some relativistic corrections can be included in a nonrelativistic treatment, but a fully relativistic model is needed for the analysis of the data at higher energies that are now becoming available. It is thus important to establish a clear relationship between the nonrelativistic DWIA treatment that was extensively used in the analysis of low-energy data and RDWIA treatments, in order to understand the relevance of genuine relativistic effects and the limit of validity of the nonrelativistic model.

Relativistic effects as well as the differences between relativistic and nonrelativistic calculations have been widely and carefully investigated in different papers where RDWIA treatments have been developed. The differences, however, were usually investigated starting from the basis of a relativistic model where terms corresponding to relativistic effects are cancelled, such as, for instance, the lower components in the Dirac spinor and the Darwin factor, or where nonrelativistic approximations are included. Although very interesting, these investigations do not correspond to the result of a direct and consistent comparison between RDWIA and the DWIA calculations carried out with the program DWEEPY, that was used in the analysis of low-energy data. In fact, DWEEPY is based on a nonrelativistic treatment where some relativistic corrections are introduced: a relativistic kinematics is adopted and relativistic corrections at the lowest order in the inverse nucleon mass are included in the nuclear current operator [21,22], which is derived from the Foldy-Wouthuysen transformation [23]. The Darwin factor can be simply included in a nonrelativistic treatment [15], but it was not explicitly considered in the data analyses carried out with DWEEPY.

Only indirect comparison between relativistic and nonrelativistic calculations can be obtained from the available data analyses carried out with DWEEPY and in RDWIA. In fact, the two types of calculations make generally use of different optical potentials and bound state wave functions, and the difference due to the different theoretical ingredients cannot be attributed to relativity. This problem was already clear in previous investigations of relativistic effects. Various attempts were made to reproduce the conditions of a nonrelativistic calculation from a relativistic approach, but a consistent and direct comparison has not yet been achieved.

The main aim of this paper is to make clear the relationship between the DWIA approach in DWEEPY and RDWIA treatments, and to investigate the relevance of genuine relativistic effects through a direct comparison between the results of the two calculations. A fully relativistic RDWIA treatment of the $(e, e'p)$ knockout reaction has thus been developed. The effective Pauli reduction [12] has been adopted for the scattering state. For the bound state the numerical solution of the Dirac equation has been used, as in this case it does not represent a too difficult problem. Various computer programs are in fact available, able to explain the global and s.p. properties of a nucleus within the framework of a relativistic mean-field theory. For the scattering state, where a partial-wave expansion is performed, the effective Pauli reduction appears simpler and more flexible, and it is equivalent to the solution of the Dirac equation. From this point of view, our relativistic approach does not contain approximations, since the Schrödinger-like equation is solved for each partial wave starting from a relativistic optical potential and without assuming the EMA prescription in the effective current operator.

The numerical results of this RDWIA model have been compared with the results of DWEEPY. A consistent comparison requires the same kinematical conditions and the use of consistent theoretical ingredients in the two calculations. Thus, in DWEEPY we have adopted for the bound state the normalized upper component of the Dirac spinor and for the scattering state the solution of the same Schrödinger-equivalent optical potential of the relativistic calculation.

Different kinematics have been considered for the comparison, with the aim to investigate the relevance of relativistic effects not included in DWEEPY in different situations, at low energy, in the kinematical region where DWEEPY was extensively and successfully applied, and at higher energy, where relativistic effects are more evident, in order to establish the limit of validity of the nonrelativistic approach.

The relevant formalism is outlined in Sec. II. Relativistic and nonrelativistic calculations of the cross section and response functions for the $^{16}\text{O}(e, e'p)$ reaction are compared in Sec. III, where various relativistic effects are investigated. Even though the comparison with experimental data is not the main aim of this work, in Sec. IV we check the reliability of our approach in comparison with data. Some conclusions are drawn in Sec. V.

II. FORMALISM

A. Relativistic current

In the one-photon exchange approximation, where a photon is exchanged between the incident electron and the target nucleus, the coincidence cross section of the $(e, e'p)$ reaction is given by the contraction between the lepton tensor, dependent only on the electron variables and completely determined by QED, and the hadron tensor, whose components are given by bilinear products of the transition matrix elements of the nuclear current operator. According to the impulse approximation, in which only one nucleon of the target is involved in the reaction, the nuclear current is assumed to be a one-body operator.

In RDWIA the matrix elements of the nuclear current operator, i.e.

$$J^\mu = \int d\mathbf{r} \bar{\Psi}_f(\mathbf{r}) \hat{j}^\mu \exp\{i\mathbf{q} \cdot \mathbf{r}\} \Psi_i(\mathbf{r}), \quad (1)$$

are calculated with relativistic wave functions for initial bound and final scattering states.

We choose the electromagnetic current operator corresponding to the *cc2* definition of Ref. [24], i.e.

$$\hat{j}^\mu = F_1(Q^2)\gamma^\mu + i\frac{\kappa}{2M}F_2(Q^2)\sigma^{\mu\nu}q_\nu, \quad (2)$$

where $q^\nu = (\omega, \mathbf{q})$ is the four-momentum transfer, $Q^2 = q^2 - \omega^2$, F_1 and F_2 are Dirac and Pauli nucleon form factors, κ is the anomalous part of the magnetic moment, and $\sigma^{\mu\nu} = i/2 [\gamma^\mu, \gamma^\nu]$. Current conservation is restored by replacing the longitudinal current by

$$J^L = J^z = \frac{\omega}{q}J^0. \quad (3)$$

In our reference frame the z -axis is along \mathbf{q} and the y -axis parallel to $\mathbf{q} \times \mathbf{p}'$.

The bound state wave function

$$\Psi_i = \begin{pmatrix} u_i \\ v_i \end{pmatrix} \quad (4)$$

is obtained as the Dirac-Hartree solution from a relativistic Lagrangian with scalar and vector potentials. Several computer codes calculating the ground and excited state properties of nuclei are easily available in literature [25,26].

The ejectile wave function is obtained following the direct Pauli reduction method. It is well known that a Dirac spinor

$$\Psi = \begin{pmatrix} \Psi_+ \\ \Psi_- \end{pmatrix} \quad (5)$$

can be written in terms of its positive energy component Ψ_+ as

$$\Psi = \begin{pmatrix} \Psi_+ \\ \frac{\boldsymbol{\sigma} \cdot \mathbf{p}}{E+M+S-V} \Psi_+ \end{pmatrix}, \quad (6)$$

where $S = S(r)$ and $V = V(r)$ are the scalar and vector potentials for the nucleon with energy E . The upper component Ψ_+ can be related to a Schrödinger-like wave function Φ by the Darwin factor $D(r)$, i.e.

$$\Psi_+ = \sqrt{D(r)} \Phi, \quad (7)$$

$$D(r) = \frac{E + M + S(r) - V(r)}{E + M}. \quad (8)$$

The two-component wave function Φ is solution of a Schrödinger equation containing equivalent central and spin-orbit potentials, which are functions of the scalar and vector potentials S and V and are energy dependent.

Inserting Eq. (7) into Eq. (6) and using the relativistic normalization, we obtain the wave function for the knocked out nucleon

$$\begin{aligned} \bar{\Psi}_f &= \Psi_f^\dagger \gamma^0 = \sqrt{\frac{E' + M}{2E'}} \left[\left(\frac{\boldsymbol{\sigma} \cdot \mathbf{p}}{C} \right) \sqrt{D} \Phi_f \right]^\dagger \gamma^0 \\ &= \sqrt{\frac{E' + M}{2E'}} \Phi_f^\dagger \left(\sqrt{D} \right)^\dagger \left(1 ; \boldsymbol{\sigma} \cdot \mathbf{p} \frac{1}{C^\dagger} \right) \gamma^0, \end{aligned} \quad (9)$$

where

$$C(r) = E' + M + S(r) - V(r). \quad (10)$$

If we substitute Eqs. (2), (4), and (9) into Eq. (1), we obtain the relativistic nuclear current

$$\begin{aligned} J^0 &= \sqrt{\frac{E' + M}{2E'}} \int d\mathbf{r} \Phi_f^\dagger \left(\sqrt{D} \right)^\dagger \left\{ F_1 \left[u_i - i\boldsymbol{\sigma} \cdot \nabla \frac{1}{C^\dagger} v_i \right] \right. \\ &\quad \left. + \frac{\kappa}{2M} F_2 \left[i(\boldsymbol{\sigma} \cdot \nabla) \frac{1}{C^\dagger} (\boldsymbol{\sigma} \cdot \mathbf{q}) u_i + \boldsymbol{\sigma} \cdot \mathbf{q} v_i \right] \right\} \exp\{i\mathbf{q} \cdot \mathbf{r}\}, \\ \mathbf{J} &= \sqrt{\frac{E' + M}{2E'}} \int d\mathbf{r} \Phi_f^\dagger \left(\sqrt{D} \right)^\dagger \left\{ F_1 \left[-i(\boldsymbol{\sigma} \cdot \nabla) \frac{1}{C^\dagger} \boldsymbol{\sigma} u_i + \boldsymbol{\sigma} v_i \right] \right. \\ &\quad \left. + i\frac{\kappa}{2M} F_2 \left[\boldsymbol{\sigma} \times \mathbf{q} u_i + \omega(\boldsymbol{\sigma} \cdot \nabla) \frac{1}{C^\dagger} \boldsymbol{\sigma} u_i \right. \right. \\ &\quad \left. \left. - i\omega \boldsymbol{\sigma} v_i + i(\boldsymbol{\sigma} \cdot \nabla) \frac{1}{C^\dagger} (\boldsymbol{\sigma} \times \mathbf{q}) v_i \right] \right\} \exp\{i\mathbf{q} \cdot \mathbf{r}\}, \end{aligned} \quad (11)$$

where the operator \mathbf{p} has been replaced by the gradient $-i\nabla$, which operates not only on the components of the Dirac spinor but also on $\exp\{i\mathbf{q} \cdot \mathbf{r}\}$.

B. Nonrelativistic current

In nonrelativistic DWIA the matrix elements of the nuclear current are

$$J_{nr}^\mu = \int d\mathbf{r} \Phi_f^\dagger(\mathbf{r}) \hat{j}_{nr}^\mu \exp\{i\mathbf{q} \cdot \mathbf{r}\} \Phi_i(\mathbf{r}), \quad (12)$$

where the bound and scattering states are eigenfunctions of a Schrödinger equation.

In standard DWIA analyses phenomenological ingredients are usually adopted for $\Phi_i(\mathbf{r})$ and $\Phi_f(\mathbf{r})$. In this work and in order to perform a consistent comparison with RDWIA calculations, we employ for $\Phi_i(\mathbf{r})$ the upper component of the Dirac wave function u_i and for $\Phi_f(\mathbf{r})$ the Schrödinger-like wave function that appear in the relativistic current of Eq. (11).

The nuclear current operator is obtained from the Foldy-Wouthuysen reduction of the free-nucleon Dirac current through an expansion in a power series of $1/M$, i.e.

$$\hat{j}_{nr}^\mu = \sum_{n=0}^N \hat{j}_{(n)}^\mu. \quad (13)$$

In the program DWEEPY the expansion is truncated at second order ($N = 2$).

C. Cross section and response functions

The coincidence cross section of the unpolarized ($e, e'p$) reaction is written in terms of four nuclear structure functions $f_{\lambda\lambda'}$ [3] as

$$\sigma_0 = \sigma_M E' |\mathbf{p}'| \left\{ \rho_{00} f_{00} + \rho_{11} f_{11} + \rho_{01} f_{01} \cos \alpha + \rho_{1-1} f_{1-1} \cos 2\alpha \right\}, \quad (14)$$

where σ_M is the Mott cross section and α the out of plane angle between the electron-scattering plane and the $(\mathbf{q}, \mathbf{p}')$ -plane. The coefficients $\rho_{\lambda\lambda'}$ are obtained from the components of the lepton tensor and depend only on the electron kinematics. The structure functions $f_{\lambda\lambda'}$ are given by suitable combinations of the components of the nuclear current as

$$\begin{aligned} f_{00} &= \langle J^0 (J^0)^\dagger \rangle, \\ f_{11} &= \langle J^x (J^x)^\dagger \rangle + \langle J^y (J^y)^\dagger \rangle, \\ f_{01} &= -2\sqrt{2} \Re \left[\langle J^x (J^0)^\dagger \rangle \right], \\ f_{1-1} &= \langle J^y (J^y)^\dagger \rangle - \langle J^x (J^x)^\dagger \rangle, \end{aligned} \quad (15)$$

where the brackets mean that the matrix elements are averaged over the initial and summed over the final states fulfilling energy conservation.

In the following we use a different definition of the structure functions, that is

$$\begin{aligned} R_L &= (2\pi)^3 f_{00}, & R_T &= (2\pi)^3 f_{11}, \\ R_{LT} &= \frac{(2\pi)^3}{\sqrt{2}} f_{01}, & R_{TT} &= -(2\pi)^3 f_{1-1}. \end{aligned} \quad (16)$$

If the electron beam is longitudinally polarized with helicity h , the coincidence cross section for a knocked out nucleon with spin directed along $\hat{\mathbf{s}}$ can be written as [3]

$$\sigma_{h,\hat{\mathbf{s}}} = \frac{1}{2} \sigma_0 \left[1 + \mathbf{P} \cdot \hat{\mathbf{s}} + h \left(A + \mathbf{P}' \cdot \hat{\mathbf{s}} \right) \right], \quad (17)$$

where σ_0 is the unpolarized cross section of Eq. (14), \mathbf{P} the induced polarization, A the electron analyzing power and \mathbf{P}' the polarization transfer coefficient. We choose for the polarimeter the three perpendicular directions: \mathbf{L} parallel to \mathbf{p}' , \mathbf{N} along $\mathbf{q} \times \mathbf{p}'$, and $\mathbf{T} = \mathbf{N} \times \mathbf{L}$. The corresponding polarization observables can be written in terms of new structure functions, which contain explicitly the polarization direction of the emitted nucleon. In coplanar kinematics ($\alpha = 0, \pi$), only P^N , P'^L , and P'^T survive [3].

III. RELATIVISTIC EFFECTS IN THE $^{16}\text{O}(e, e'p)$ REACTION

The reaction $^{16}\text{O}(e, e'p)^{15}\text{N}$ has been chosen as a well suited process for testing the relativistic program and investigating the differences with respect to the nonrelativistic program DWEEPY [7]. A large experience concerning theoretical calculations is available on this reaction and a considerable amount of experimental data at different energies and kinematics has been published, including polarization measurements.

The relativistic bound-state wave functions used in the calculations have been obtained from the program ADFX of Ref. [26], where relativistic Hartree-Bogoliubov equations are solved. The model is applied in the mean-field approximation to the description of ground-state properties of spherical nuclei [27]. Sigma-meson, omega-meson, rho-meson and photon field contribute to the interaction and their potentials are obtained by solving self-consistently Klein-Gordon equations. Moreover, finite range interactions are included to describe pairing correlations and the coupling to particle continuum states. The corresponding wave function for the nonrelativistic calculation has been taken as the upper component of the relativistic Dirac four-component spinor with the proper normalization, i.e. normalized to one in the coordinate and spin space. This is not the best choice for DWEEPY, but a consistent use of the theoretical ingredients is necessary to allow a clear comparison between the two approaches.

The relativistic nuclear current was taken as in Eq. (2) [24]. This expression is not only more fundamental than the other forms recovered from the Gordon decomposition, but it is also consistent with the nonrelativistic current used

in DWEEPY, where the relativistic corrections up to order $1/M^2$ are obtained from a Foldy-Wouthuysen transformation applied to the interaction Hamiltonian where the nuclear current has the same form as in Eq. (2). The Dirac and Pauli form factors F_1 and F_2 are taken in both calculations from Ref. [28].

The outgoing-proton wave function is calculated by means of the relativistic energy-dependent optical potential of Ref. [29], which fits proton elastic scattering data on several nuclei in an energy range up to 1040 MeV. The program GLOBAL of Ref. [29], which generates the scalar and vector components of the Dirac optical potential, has been used. Different fits, available from the code, were explored. The Schrödinger equivalent potentials calculated in the same program were used for the nonrelativistic calculation.

The comparison between the results of the two approaches is not restricted to the cross section, but involves also the structure functions, which can be experimentally separated and show a different sensitivity to the treatment of the theoretical ingredients and to relativistic effects.

A kinematics with constant (\mathbf{q}, ω) , or perpendicular kinematics, was chosen as convenient for the comparison, but some calculations were performed also in parallel kinematics. In both kinematics the incident electron energy and the outgoing proton energy are fixed. In the kinematics with constant (\mathbf{q}, ω) the electron scattering angle is calculated by imposing the condition $|\mathbf{q}| = |\mathbf{p}'|$. Changing the angle of the outgoing proton, different values of the recoil or missing momentum p_m , with $\mathbf{p}_m = \mathbf{q} - \mathbf{p}'$, can be explored. In parallel kinematics \mathbf{q} is parallel or antiparallel to \mathbf{p}' , and different values of p_m are obtained changing the electron scattering angle, and thus \mathbf{q} .

The beam energy E_0 was fixed in the present work at 2 GeV, in order to minimize the effect of the Coulomb distortion, which is included in the relativistic program only through the effective momentum approximation [3,7]. Calculations were performed for an outgoing proton energy up to 400 MeV. The missing momentum was explored in a range up to ~ 400 MeV/ c .

A. Relativistic *vs* nonrelativistic results

In this Section the results of the comparison between the DWIA calculations performed with DWEEPY and RDWIA calculations are discussed. DWEEPY is based on a nonrelativistic treatment, but does already contain some relativistic corrections in the kinematics and in the nuclear current through the expansion in $1/M$. Therefore, the results of DWEEPY cannot be obtained from the relativistic program simply by dropping relativistic effects, such as the lower components of the Dirac spinor and applying the proper normalizations. Here the comparison is done between the results of the two independent programs. In the first place we checked the numerical consistency of the two programs and verified that they give the same result in the same situation, i.e. when all the differences are eliminated. This numerical check gives us confidence that we are not interpreting the contribution of different ingredients as a relativistic effect.

The comparison between the results of the new RDWIA program and DWEEPY is shown in Figs. 1–6, for the structure functions and the cross section of the $^{16}\text{O}(e, e'p)^{15}\text{N}_{\text{g.s.}}$ reaction in a kinematics with constant (\mathbf{q}, ω) , at three values of the proton energy, i.e. $T_p = 100$ MeV, 200 MeV and 300 MeV.

It is clear from these figures that the differences rapidly increase with the energy. Moreover, the relativistic result is smaller than the nonrelativistic one. This is a well known effect, which was found in all the relativistic calculations and which is essentially due to the Darwin factor [15] of Eq. (8). In addition, the relativistic calculations include the typical normalization factor $(E + M)/2E$ (see Eq. (9)), which has the value 0.95 at 100 MeV and decreases to 0.87 at 300 MeV.

A significant difference is found for the transverse structure function R_T even at $T_p = 100$ MeV, where a reduction of about 15% is obtained with respect to the nonrelativistic calculation. The reduction grows up to about 25% at 200 MeV, and 40% at 300 MeV. The difference is sensibly reduced, mainly at lower energies, by including in the nuclear current the terms to the order $1/M^3$.

Only small differences are found for the longitudinal structure function R_L at all the considered proton energies. Its size, however, decreases when the energy increases and therefore its contribution to the cross section becomes less important.

Large differences are generally found for the interference structure function R_{LT} . The combined relativistic effects on R_T and R_{LT} are responsible for the different asymmetry in the cross section at positive and negative values of p_m , where the mismatch between the two structure functions adds up on the one side and compensates on the other side.

Large relativistic effects are also found on R_{TT} , which is anyhow much smaller than the other structure functions and gives only a negligible contribution to the cross section.

As relativistic effects increase with the energy, the conclusion of this comparison is that DWEEPY can be used with enough confidence at energies around 100 MeV, and, with some caution, up to about 200 MeV. Higher-order terms in the nuclear current can account for a part of the difference in this kinematical region. A fully relativistic calculation is

anyhow convenient at 200 MeV and necessary above 300 MeV. This result is consistent with the old one of Ref. [22], where the validity of the relativistic corrections to the nuclear current, calculated as an expansion on $1/M$, were discussed and an upper limit of $|\mathbf{q}| \sim 600$ MeV/ c was stated for the nonrelativistic calculations.

A calculation was performed also in parallel kinematics at $T_p = 100$ and 200 MeV. In this kinematics only the longitudinal R_L and the transverse structure function R_T survive. The results are shown in Figs. 7 and 8. Also in this case small differences are found for R_L , while R_T is significantly reduced in RDWIA. The reduction increases with the outgoing proton energy, and, at a given values of T_p , is larger at positive p_m , when the momentum transfer decreases. This is mainly due to the fact that the leading term of the spin current, proportional to \mathbf{q} , is the same in the relativistic and nonrelativistic expressions.

B. Darwin factor and spinor distortion of the scattering state

In this Section we shall discuss the effect of the optical potential in the Pauli reduction of the four-component Dirac spinor for the scattering state. We do not discuss the corresponding effect on the bound state, as in our calculations the bound-state wave function is taken directly from the solution of the relativistic Dirac equation.

The effect of the optical potential on the Pauli reduction is twofold: the Darwin factor $D(r)$ of Eq. (8), which directly multiplies the Schrödinger-equivalent eigenfunction, and the spinor distortion $C(r)$ of Eq. (10), which applies only to the lower component of the Dirac spinor. The distortion of the scattering wavefunction, which is calculated through a partial wave expansion, is always included in the calculation and affects in a similar way the relativistic and nonrelativistic result.

The Darwin factor gives a reduction of about 5-10% at 100 MeV, which is consistent with the qualitative prediction of Ref. [15]. On the contrary, spinor distortion produces an enhancement of the cross section, so that the combined effect of the two corrections is in general small. Moreover, it decreases with the energy. The result is qualitatively in agreement with the ones of Ref. [11,20].

In Figs. 9 and 10 the comparison between the two results is shown in the kinematics with constant (\mathbf{q}, ω) at $T_p = 100$ MeV, for the structure functions and the cross section, respectively. The effect is always small. Spinor distortion enhances the cross section at high and negative recoil momenta, but this effect seems absent at $p_m > 0$ or it is pushed to very high momenta.

The effect is larger on R_L than on R_T . Thus, at higher energies, where R_T becomes larger than R_L , the effect of spinor distortion on the cross section decreases.

C. Effective momentum approximation

In this Section the validity of EMA is discussed. This prescription, which consists in evaluating the momentum operator in the effective nuclear current using the asymptotic value of the outgoing proton momentum, simplifies considerably the numerical calculations, avoiding the evaluation of the gradient in Eq. (11). It is exact in plane wave impulse approximation (PWIA), where the scattering wave functions are eigenfunctions of the momentum, but in DWIA it disregards the spreading of the distorted proton wave function in momentum space due to FSI.

This approximation was used in some relativistic calculations, and in particular in the model of Refs. [19,20] for bound and scattering states. Since in our approach the bound-state wave function is taken directly from the solution of the Dirac equation, we investigate the validity of EMA only for the scattering state.

We have to notice that in our calculations EMA does not change the nuclear current operator, which is calculated with the $cc2$ formula and therefore does not depend on the momentum. The only dependence is contained in the Pauli reduction of the scattering wave function.

The effect of EMA in our RDWIA approach is shown in Figs. 9 and 10, where the the structure functions and the cross section calculated with EMA in the kinematics with constant (\mathbf{q}, ω) at $T_p = 100$ MeV are displayed and compared with the exact result. At 100 MeV the difference is indeed sensible, but it rapidly decreases with the energy. At 200 MeV it is much smaller, and becomes really negligible at ~ 400 MeV, and therefore at the energy of the TJNAF experiment. This behaviour can be understood if one considers that distortion effects decrease with the energy, so that at high energy DWIA approaches the PWIA result, where EMA is exact.

IV. COMPARISON WITH EXPERIMENTAL DATA

In this Section we shall discuss the comparison of our RDWIA results with experimental data. Data are available at low energies, where DWEOPY was extensively and successfully applied, and, more recently, at higher energies, where other RDWIA calculations have given an excellent agreement. Even though a precise description of experimental data is not the main aim of this work, it is interesting to test the predictions of our relativistic approach in comparison with data that have been already and successfully described by other theoretical models.

A. The $^{16}\text{O}(e, e'p)$ reaction

Low-energy data are presented in terms of the reduced cross section [3], which is defined as the cross section divided by a kinematical factor and the elementary off-shell electron-proton scattering cross section, usually σ_{cc1} of Ref. [24].

In Fig. 11 the reduced cross sections measured at NIKHEF [30] for the $^{16}\text{O}(e, e'p)$ knockout reaction and for the transitions to the $1/2^-$ ground state and the $3/2^-$ excited state of ^{15}N are displayed and compared with the results given by our RDWIA program and by DWEOPY. The experiment was carried out in parallel kinematics at $T_p = 90$ MeV.

The relativistic results are lower than the nonrelativistic ones and the corresponding spectroscopic factors are approximately 10% larger than those deduced from nonrelativistic analyses. Thus, the normalization (spectroscopic) factor, applied in Fig. 11 to the calculated results in order to reproduce the size of the experimental data, is 0.70 for RDWIA and 0.65 for DWEOPY. The same value is adopted for the two final states.

As we already stated in Sec. III, only small differences are found at this proton energy between the two models. Thus, the results of the two calculations are almost equivalent in comparison with data, which are reasonably described by both calculations. A better agreement is found for the $1/2^-$ than for the $3/2^-$ state. In any case, it is not as good as in the DWIA analysis of Ref. [30] performed with DWEOPY. This result is expected, as we already claimed that the theoretical ingredients, bound state and optical potential, used in the present calculation do not represent the best choice for DWEOPY, but are here adopted in order to allow a consistent comparison between the relativistic and nonrelativistic approaches.

In Figs. 12–15 the cross sections and the structure functions measured at TJNAF [16] for the $^{16}\text{O}(e, e'p)$ knockout reaction and for the transitions to the $1/2^-$ ground state and the $3/2^-$ excited state of ^{15}N are displayed and compared with the results of our RDWIA model. The experiment was carried out in a kinematics with constant (\mathbf{q}, ω) , with $E_0 = 2.4$ GeV and $\omega \sim 439$ MeV. Only RDWIA calculations are shown in the figure, since we know from the investigation of Sec. III that at the proton energy of this experiment relativistic effects are large and a relativistic analysis is necessary. In order to study the sensitivity to different optical potentials, we compare in the figures results obtained with the EDAD1 and EDAL-O fits of Ref. [29]. Only small differences are given by the two optical potentials. The agreement with data is satisfactory and of about the same quality as in other RDWIA analyses, but for the interference structure function R_{LT} for the $1/2^-$ state at intermediate missing momenta. A better description of data might be obtained with a more careful determination of the theoretical ingredients.

It is interesting to notice that the spectroscopic factor applied to all the calculations in Figs. 12–15 is the same, i.e. 0.7, as that found in the comparison with NIKHEF data shown in Fig. 11. A spectroscopic factor of about 0.7 was also obtained in previous RDWIA analyses of the same TJNAF data [16].

B. The $^{12}\text{C}(e, e'\vec{p})$ and $^{16}\text{O}(\vec{e}, e'\vec{p})$ reactions

The induced polarization of the outgoing proton P^N was measured at Bates for the $^{12}\text{C}(e, e'\vec{p})$ reaction [18]. Data were taken in a kinematics with constant (\mathbf{q}, ω) at $E_0 = 579$ MeV and $\omega \sim 290$ MeV. In Fig. 16 these data are displayed and compared with our RDWIA calculations. Results obtained with the EDAD1 and EDAL-C optical potentials are compared in the figure. The EDAD1 curve gives a better description of the experimental data at high values of the missing momentum, but both calculations are in fair agreement with data. With EDAD1 potential, we also plot results after eliminating the negative energy components in the bound state.

As already shown in Ref. [11] the polarization P^N is enhanced by the presence of the negative energy components of the relativistic bound state wave function. This result is confirmed in Fig. 16 by the dashed line which gives a smaller P^N .

A slightly higher polarization is obtained in Ref. [11] with the nuclear current written in the $cc1$ form according to Ref. [24].

The components of the polarization coefficient P'^L and P'^S were measured at TJNAF [17] for the $^{16}\text{O}(\bar{e}, e'\bar{p})$ reaction and for the transitions to the $1/2^-$ ground state and the $3/2^-$ excited state of ^{15}N . The experiment was performed in the same kinematics as in Ref. [16], that is the one of Figs. 12–15. The experimental data are compared with our RDWIA calculations in Fig. 17 for $1/2^-$ and in Fig. 18 for the $3/2^-$ state. The two curves in the figures show the results obtained with the EDAD1 and EDAI-O fits. Both results are in satisfactory agreement with data.

V. SUMMARY AND CONCLUSIONS

In order to clarify the differences between the usual nonrelativistic approach and a relativistic description of exclusive $(e, e'p)$ knockout reactions, we have performed a fully relativistic calculation and compared it with the nonrelativistic results of the DWEEPY code, that was successfully used to analyse a large number of experimental data. The transition matrix element of the nuclear current operator is written in RDWIA using the relativistic bound state wave functions obtained in the framework of the mean field theory, and the direct Pauli reduction method with scalar and vector potentials for the ejectile wave functions. Correspondingly, the nonrelativistic DWIA matrix elements are computed in a consistent way to allow a direct comparison with the relativistic results.

The main aim of this paper was not to make a precise analysis of the existing experimental data, but to discuss the use of a nonrelativistic approach at energies higher than those generally considered up to few years ago, and to clarify the possible relativistic effects arising also at lower energies.

We have used the new RDWIA and DWEEPY codes to perform calculations for several kinematical conditions. The relativistic results are always smaller than the nonrelativistic ones and the difference increases with energy. The transverse and interference structure functions are particularly sensitive to relativistic effects, much more than the longitudinal structure function. R_T is sensibly reduced even at low energy: inclusion of higher order terms in the nonrelativistic nuclear current can reduce the difference, but a fully relativistic calculation is necessary above $T_p \sim 200$ MeV.

The effect of the scalar and vector potentials in the Pauli reduction for the scattering state has been discussed. These potentials appear in the relativistic treatment and are absent in the nonrelativistic one. The combined contribution of the reduction due to the Darwin factor and of spinor distortion, which enhances the effects of the lower components of the Dirac spinor, is always small.

The validity of EMA in the scattering state of relativistic calculations has been studied. The differences with respect to the exact results are sensible at $T_p = 100$ MeV, but rapidly decrease with the energy and become negligible at $T_p \sim 400$ MeV.

We have tested our new RDWIA calculations in comparison with experimental data that have already been described by other models. The agreement is satisfactory and comparable with other relativistic analyses.

-
- [1] S. Frullani and J. Mougey, *Adv. Nucl. Phys.* **14**, 1 (1984).
 - [2] S. Boffi, C. Giusti, and F. D. Pacati, *Phys. Rep.* **226**, 1 (1993)
 - [3] S. Boffi, C. Giusti, F. D. Pacati, and M. Radici, *Electromagnetic Response of Atomic Nuclei*, Oxford Studies in Nuclear Physics (Clarendon Press, Oxford, 1996).
 - [4] J. J. Kelly, *Adv. Nucl. Phys.* **23**, 75 (1996).
 - [5] J. Mougey *et al.* *Nucl. Phys.* **A262**, 461 (1976);
M. Bernheim *et al.* *Nucl. Phys.* **A375**, 381 (1982).
 - [6] P. K. A. de Witt Huberts, *J. Phys. G* **16**, 507 (1990);
L. Lapikás, *Nucl. Phys.* **A553**, 297c (1993).
 - [7] C. Giusti and F. D. Pacati, *Nucl. Phys.* **A473**, 717 (1987); *Nucl. Phys.* **A485**, 461 (1988).
 - [8] A. Picklesimer, J. W. Van Orden, and S. J. Wallace, *Phys. Rev. C* **32**, 1312 (1985);
A. Picklesimer and J. W. Van Orden, *Phys. Rev. C* **40**, 290 (1989).
 - [9] Y. Jin, D. S. Onley, and L. E. Wright, *Phys. Rev. C* **45**, 1311 (1992);
Y. Jin, J. K. Zhang, D. S. Onley, and L. E. Wright, *Phys. Rev. C* **47**, 2024 (1993);
Y. Jin and D. S. Onley, *Phys. Rev. C* **50**, 377 (1994).
 - [10] J. M. Udías, P. Sarriguren, E. Moya de Guerra, E. Garrido, and J. A. Caballero, *Phys. Rev. C* **48**, 2731 (1993);
J. M. Udías, P. Sarriguren, E. Moya de Guerra, and J. A. Caballero, *Phys. Rev. C* **53**, R1488 (1996);
J. M. Udías, J. A. Caballero, E. Moya de Guerra, J. E. Amaro, and T. W. Donnelly, *Phys. Rev. Lett.* **83**, 5451 (1999).

- [11] J. M. Udías and R. Vignote Phys. Rev. C **62**, 034302 (2000).
- [12] M. Hedayati-Poor, J. I. Johansson, and H. S. Sherif, Phys. Rev. C **51**, 2044 (1995).
- [13] J. I. Johansson, H. S. Sherif, and G. M. Lotz, Nucl. Phys. **A605**, 517 (1996).
- [14] J. I. Johansson and H. S. Sherif, Phys. Rev. C **59**, 3481 (1999).
- [15] S. Boffi, C. Giusti, F. D. Pacati, and F. Cannata, Nuovo Cimento **A 98**, 291 (1987).
- [16] J. Gao *et al.* Phys. Rev. Lett. **84**, 3265 (2000).
- [17] S. Malov *et al.* Phys. Rev. C **62**, 057302 (2000).
- [18] R. J. Woo *et al.* Phys. Rev. Lett. **80**, 456 (1998).
- [19] J. J. Kelly, Phys. Rev. C **56**, 2672 (1997); **59**, 3256 (1999).
- [20] J. J. Kelly, Phys. Rev. C **60**, 044609 (1999).
- [21] K. W. McVoy and L. Van Hove, Phys. Rev. **125**, 1034 (1962).
- [22] C. Giusti and F. D. Pacati, Nucl. Phys. **A336**, 427 (1980).
- [23] L. L. Foldy and S. A. Wouthuysen, Phys. Rev. **78**, 29 (1950).
- [24] T. de Forest, Jr., Nucl. Phys. **A392**, 232 (1983).
- [25] C. J. Horowitz, D. P. Murdoch, and B. D. Serot, in *Computational Nuclear Physics I: Nuclear Structure*, edited by K. Langanke, J. A. Maruhn, and S. E. Koonin (Springer-Verlag, Berlin, 1991).
- [26] W. Pöschl, D. Vretenar, and P. Ring, Comput. Phys. Commun. **103**, 217 (1997).
- [27] G. A. Lalazissis, J. König, and P. Ring, Phys. Rev. C **55**, 540 (1997).
- [28] P. Mergell, Ulf-G. Meissner, and D. Drechsel, Nucl. Phys. **A596**, 367 (1996).
- [29] E. D. Cooper, S. Hama, B. C. Clark, and R. L. Mercer, Phys. Rev. C **47**, 297 (1993).
- [30] M. Leuschner *et al.*, Phys. Rev. C **49**, 955 (1994).

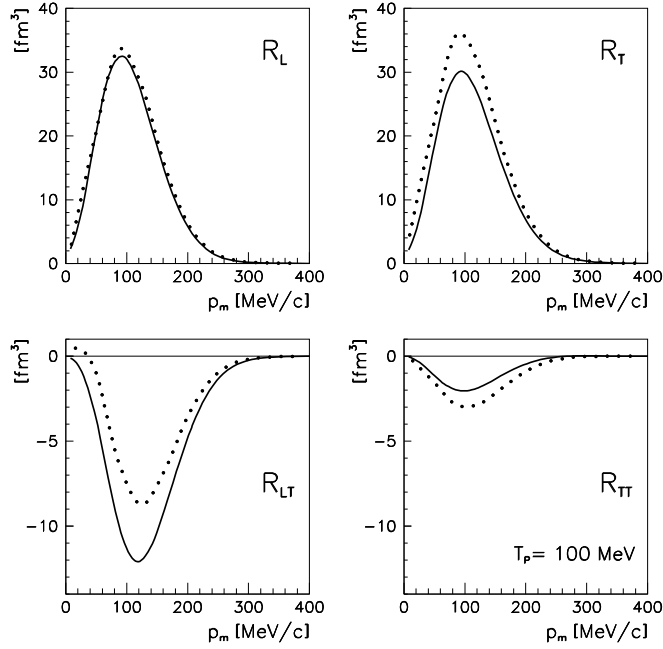


FIG. 1. The structure functions of the $^{16}\text{O}(e, e'p)$ reaction as a function of the recoil momentum p_m for the transition to the $1/2^-$ ground state of ^{15}N , in a kinematics with constant (\mathbf{q}, ω) , with $E_0 = 2000$ MeV and $T_p = 100$ MeV. The solid lines give the RDWIA result, the dotted lines the nonrelativistic result of DWEEPY. Positive (negative) values of p_m refer to situations where the angle between \mathbf{p}' and the incident electron \mathbf{k} is larger (smaller) than the angle between \mathbf{q} and \mathbf{k} .

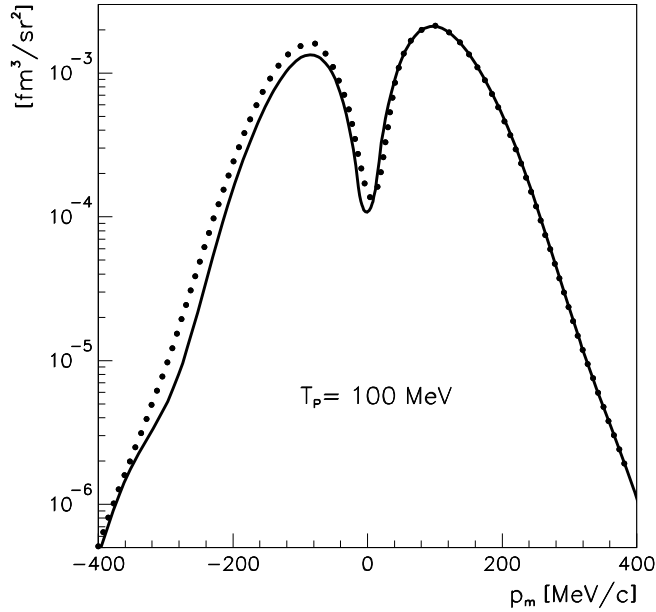


FIG. 2. The same as in Fig. 1, but for the cross section of the $^{16}\text{O}(e, e'p)$ reaction.

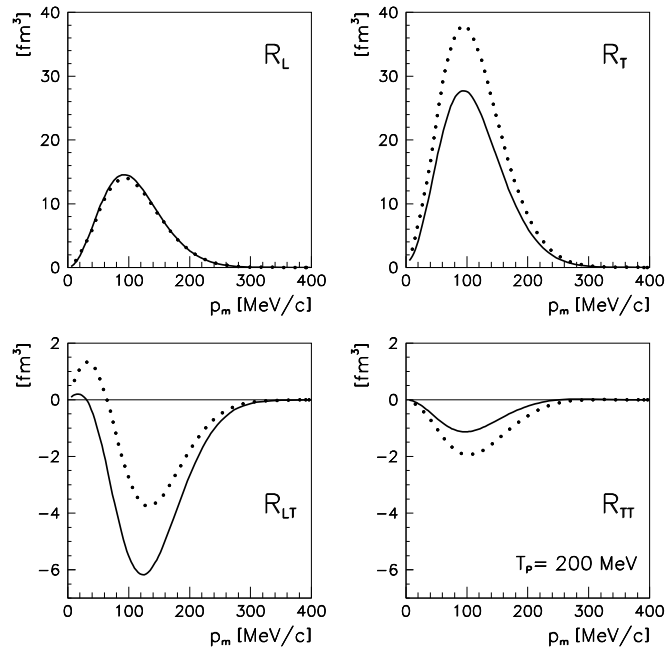


FIG. 3. The same as in Fig. 1 at $T_p = 200$ MeV.

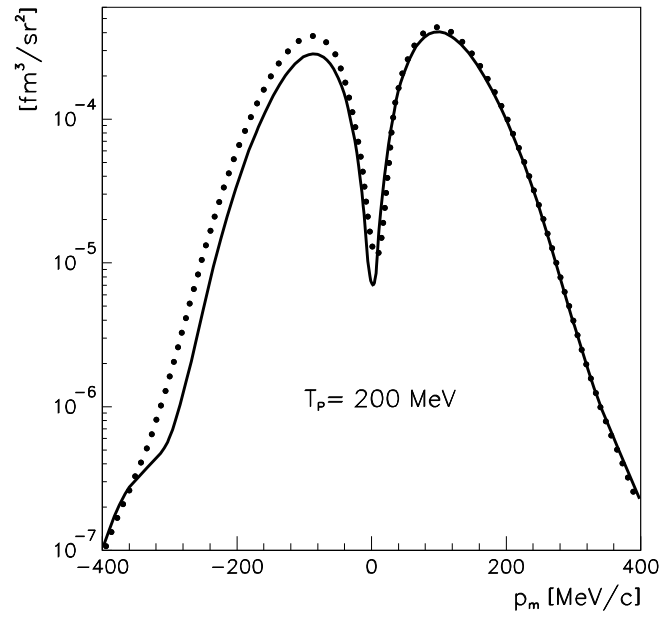


FIG. 4. The same as in Fig. 2 at $T_p = 200$ MeV.

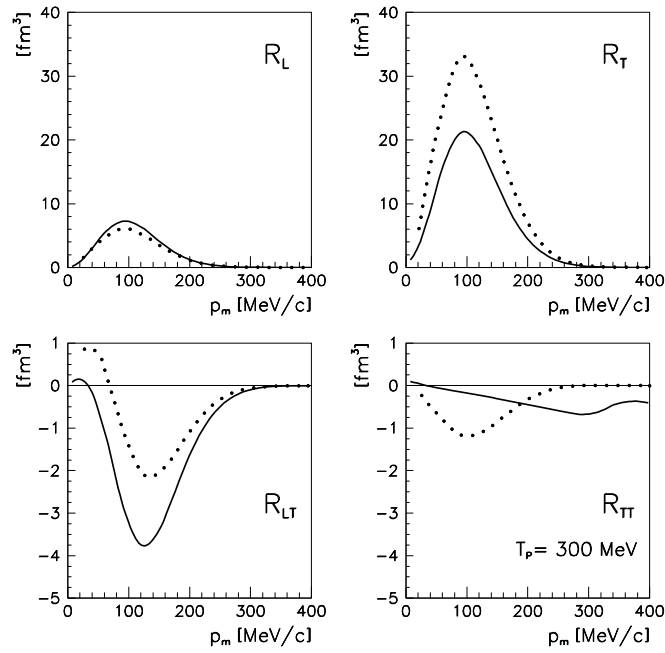


FIG. 5. The same as in Fig. 1 at $T_p = 300$ MeV.

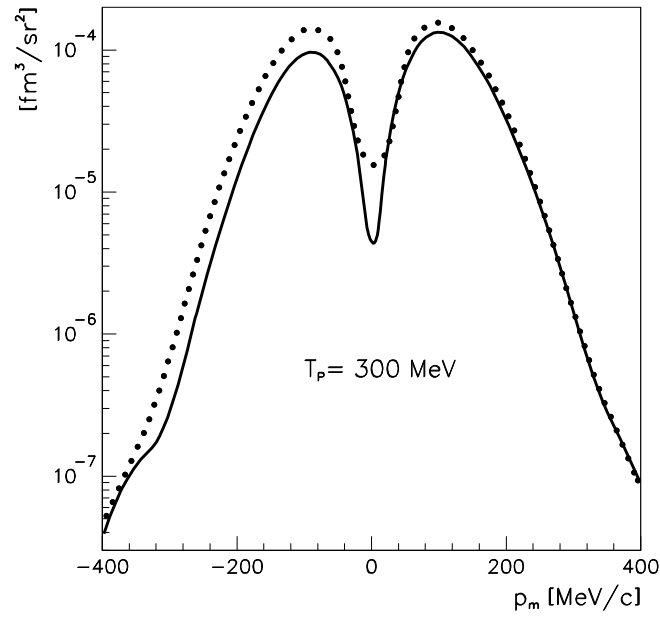


FIG. 6. The same as in Fig. 2 at $T_p = 300$ MeV.

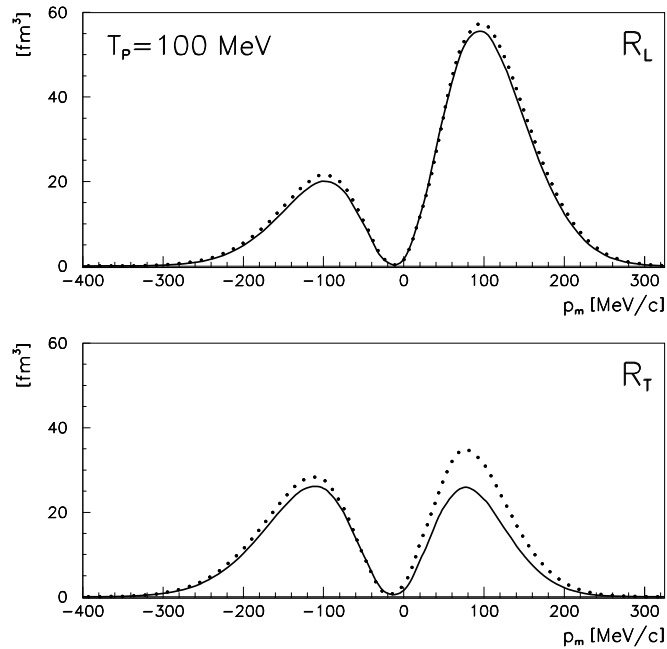


FIG. 7. The longitudinal and transverse structure functions of the $^{16}\text{O}(e, e'p)$ reaction as a function of the recoil momentum p_m for the transition to the $1/2^-$ ground state of ^{15}N , in parallel kinematics with $E_0 = 2000$ MeV and $T_p = 100$ MeV. Positive (negative) values of p_m refer to situations where $|\mathbf{p}'| > |\mathbf{q}|$ ($|\mathbf{p}'| < |\mathbf{q}|$). Line convention as in Fig. 1.

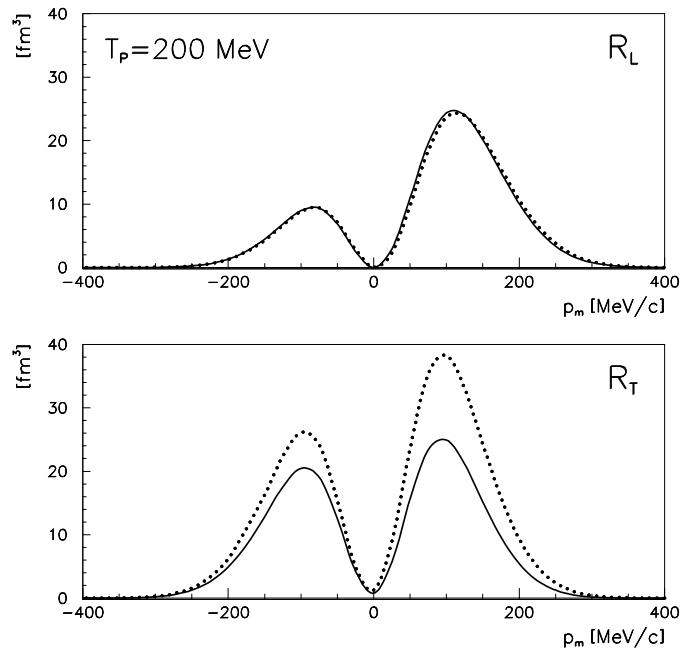


FIG. 8. The same as in Fig. 7 for $T_p = 200$ MeV.

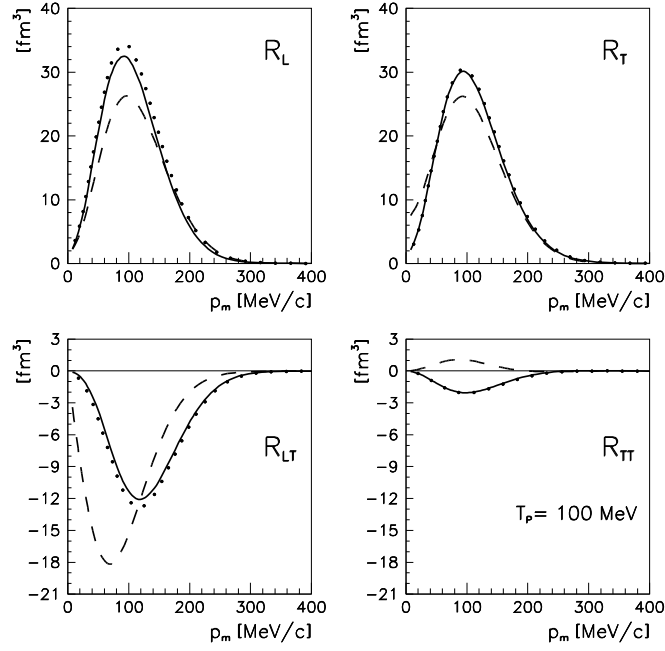


FIG. 9. The structure functions of the $^{16}\text{O}(e, e'p)$ reaction as a function of the recoil momentum p_m for the transition to the $1/2^-$ ground state of ^{15}N , in the same situation as in Fig. 1. The solid lines give the RDWIA result, the dotted lines the calculation without the Darwin factor and spinor distortion and the dashed line the EMA.

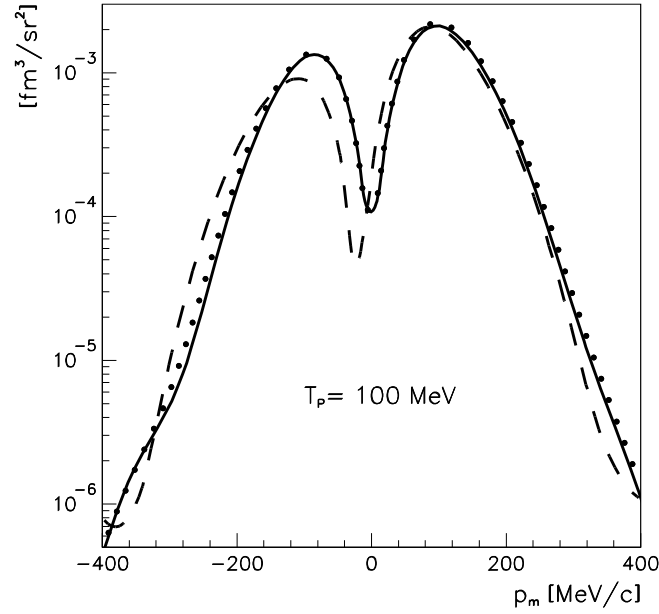


FIG. 10. The same as in Fig. 9, but for the cross section of the $^{16}\text{O}(e, e'p)$ reaction.

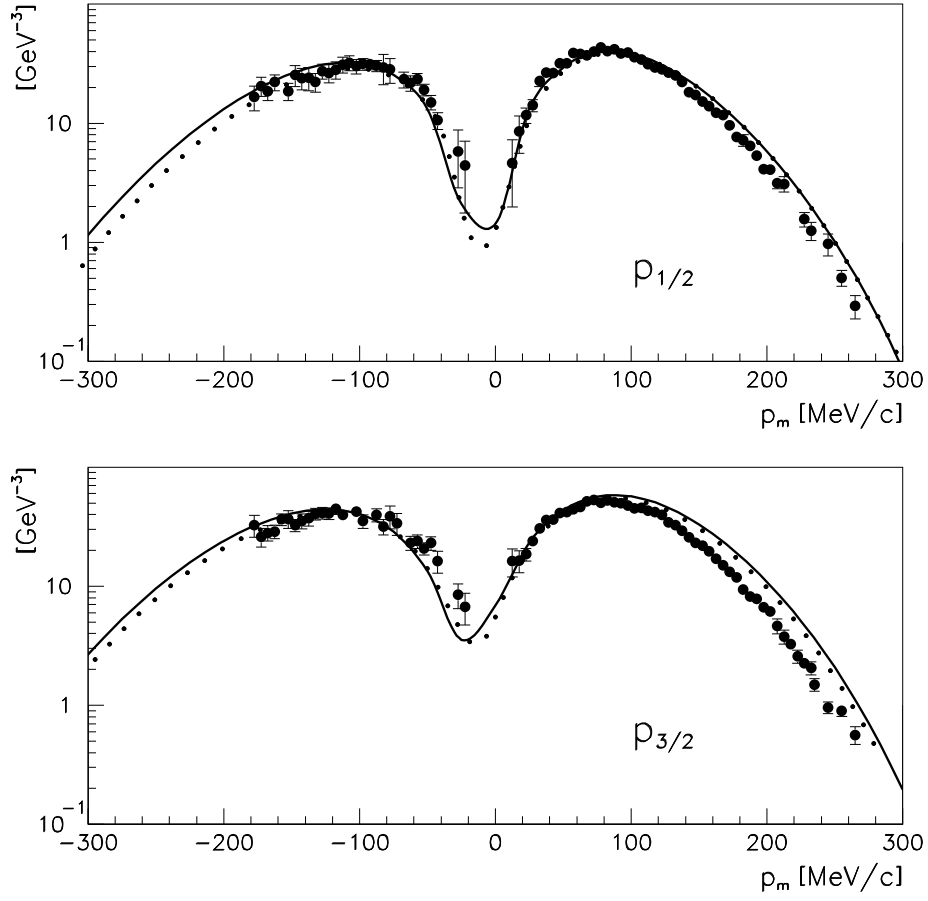


FIG. 11. The reduced cross section of the $^{16}\text{O}(e, e'p)$ reaction as a function of the recoil momentum p_m for the transitions to the $1/2^-$ ground state and to the $3/2^-$ excited state of ^{15}N , in parallel kinematics with $E_0 = 520$ MeV and $T_p = 90$ MeV. The data are from Ref. [30]. The solid lines give the RDWIA result, the dotted lines the nonrelativistic result of DWEEPY.

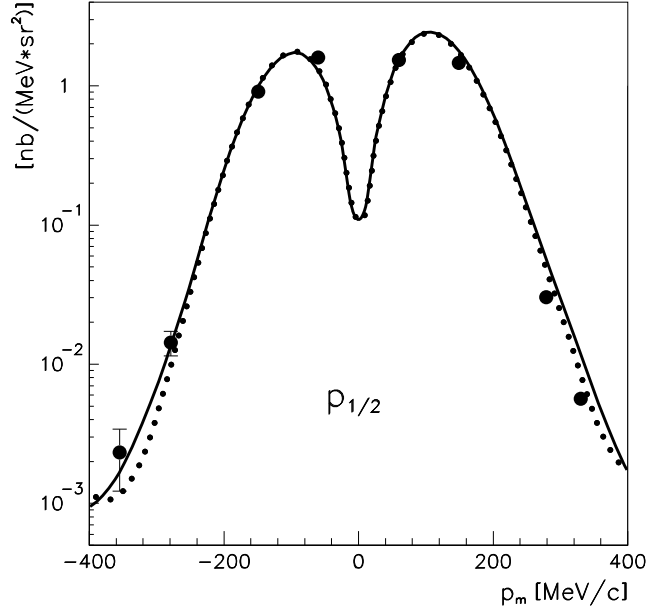


FIG. 12. The cross section of the $^{16}\text{O}(e, e'p)$ reaction as a function of the recoil momentum p_m for the transition to the $1/2^-$ ground state of ^{15}N in a kinematics with constant (q, ω) , with $E_0 = 2445$ MeV and $T_p = 433$ MeV. The data are from Ref. [16]. The solid line gives the RDWIA result with the EDAD1 optical potential, the dotted line the RDWIA result with the EDAI-O optical potential.

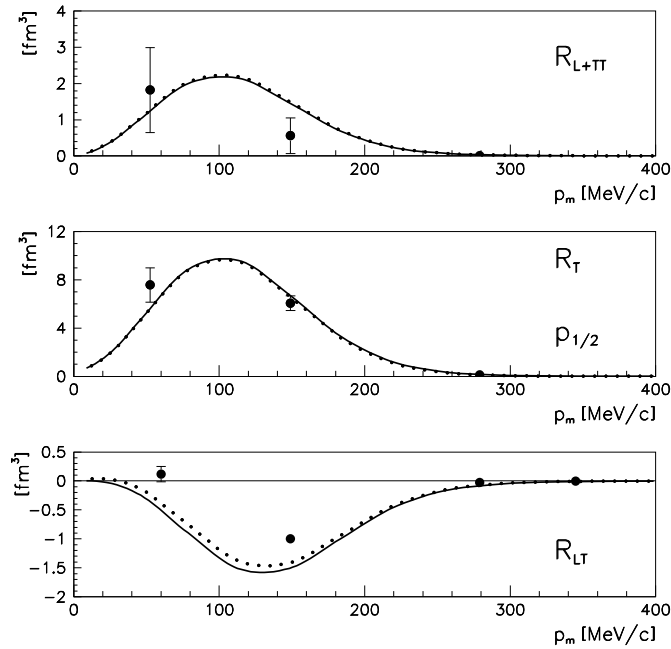


FIG. 13. The same as in Fig. 12 but for the response functions of the $^{16}\text{O}(e, e'p)$ reaction.

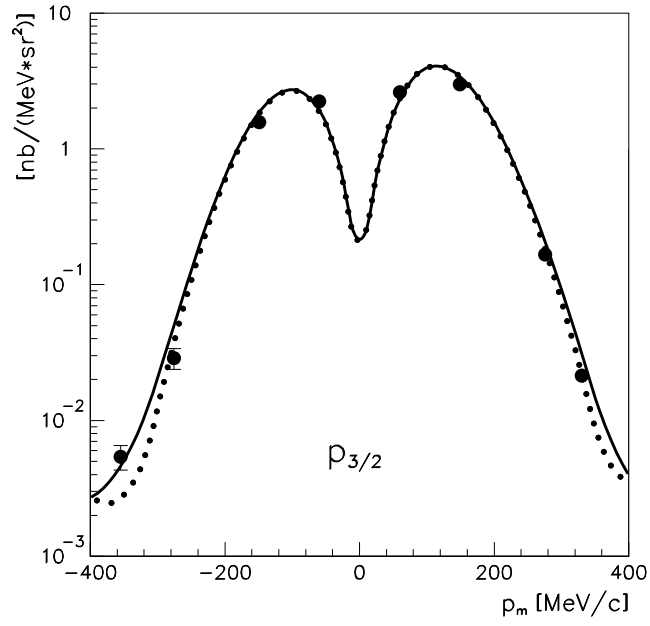


FIG. 14. The same as in Fig. 12 but for the transition to the $3/2^-$ excited state of ^{15}N .

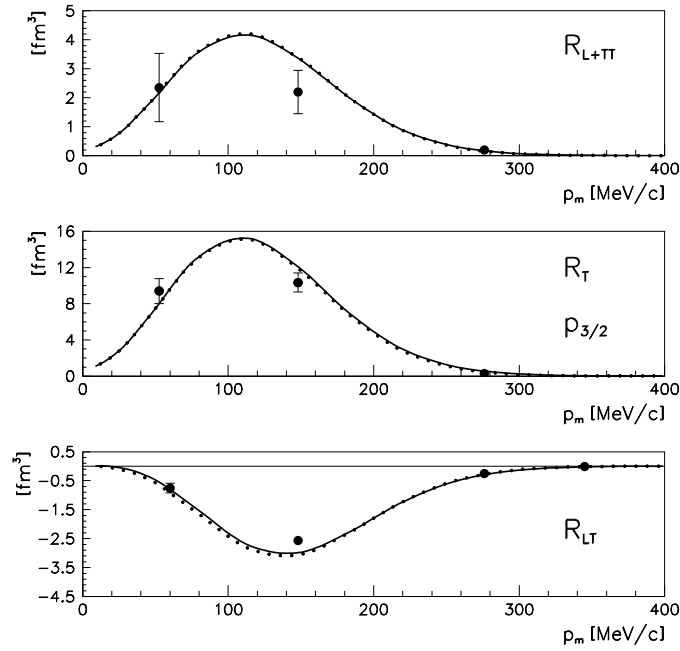


FIG. 15. The same as in Fig. 13 but for the transition to the $3/2^-$ excited state of ^{15}N .

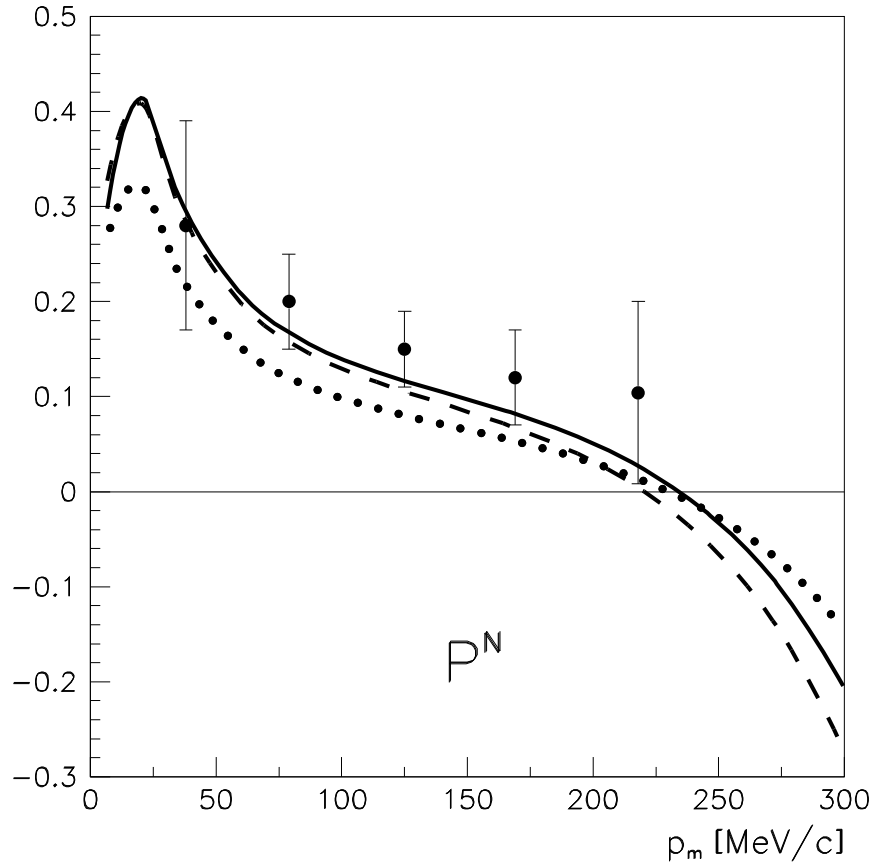


FIG. 16. The induced polarization of the emitted proton for the $^{12}\text{C}(e, e'\vec{p})$ reaction as a function of the recoil momentum p_m for the transition to the $3/2^-$ ground state of ^{11}B in a kinematics with constant (q, ω) , with $E_0 = 579$ MeV and $T_p = 274$ MeV. The data are from Ref. [18]. The solid line gives the RDWIA result with the EDAD1 optical potential, the dotted line the RDWIA result with the EDAl-C optical potential, and the dashed line the result with the EDAD1 optical potential and after removing the negative energy components in the bound state.

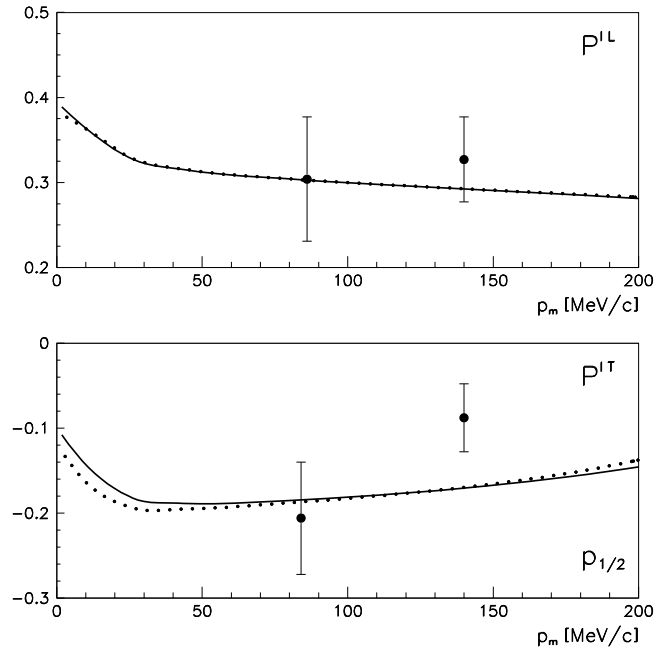


FIG. 17. The components of the polarization transfer coefficient P^L and P^T for the $^{16}\text{O}(\bar{e}, e'\bar{p})$ reaction as a function of the recoil momentum p_m for the transition to the $1/2^-$ ground state of ^{15}N in the same kinematics as in Fig. 12. The data are from Ref. [17]. The solid lines give the RDWIA result with the EDAD1 optical potential, the dotted lines the RDWIA result with the EDAI-O optical potential.

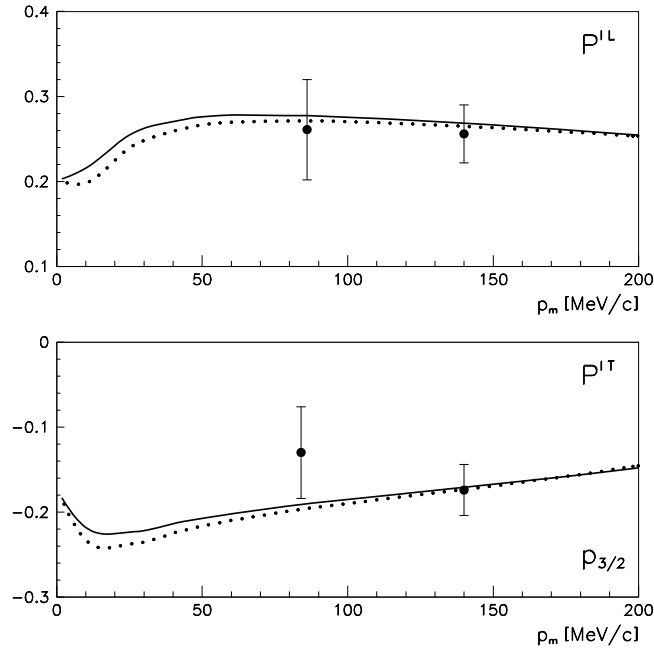


FIG. 18. The same as in Fig. 17 but for the transition to the $3/2^-$ excited state of ^{15}N .